# Figure of Merit-Based **Change Material-Based Composites for Portable Electronics Using Simplified**

# **Optimization Approach of Phase** Model This work presents an approach to optimally designing a composite with thermal conductivity enhancers infiltrated with phase change material based on figure of merit (FOM) for thermal management of portable electronic devices. The FOM defines the balance between effective thermal conductivity and energy storage capacity. In this study, thermal

conductivity enhancers are in the form of a honeycomb structure. Thermal conductivity enhancers are often used in conjunction with phase change material to enhance the conductivity of the composite medium. Under constrained heat sink volume, the higher volume fraction of thermal conductivity enhancers improves the effective thermal conductivity of the composite, while it reduces the amount of latent heat storage simultaneously. This work arrives at the optimal design of composite for electronic cooling by maximizing the FOM to resolve the stated tradeoff. In this study, the total volume of the composite and the interfacial heat transfer area between the phase change material and thermal conductivity enhancers are constrained for all design points. A benchmarked two-dimensional direct computational fluid dynamics model was employed to investigate the thermal performance of the phase change material and thermal conductivity enhancer composite. Furthermore, assuming conduction-dominated heat transfer in the composite, a simplified effective numerical model that solves the single energy equation with the effective properties of the phase change material and thermal conductivity enhancer has been developed. The effective properties like heat capacity can be obtained by volume averaging; however, effective thermal conductivity (required to calculate FOM) is unknown. The effective thermal conductivity of the composite is obtained by minimizing the error between the transient temperature gradient of direct and simplified model by iteratively varying the effective thermal conductivity. The FOM is maximized to find the optimal volume fraction for the present design. [DOI: 10.1115/1.4052074] change materials (PCMs) for thermal management of such devices has been proposed and studied widely. Increased functionalities in the portable electronic devices lead to intermittent chip power surges that stay for a prolonged time in a very small chip area. The intermittent power load happens for a short time (thermal spike) in most of the smartphone applications, i.e., they operate for a short period of time and remain idle for some time before another thermal spike. For improvement in the

# Ayushman Singh

Department of Mechanical Engineering, State University of New York at Binghamton, Vestal, NY 13850

# Srikanth Rangarajan

Department of Mechanical Engineering, State University of New York at Binghamton, Vestal, NY 13850 e-mail: srangar@binghamton.edu

# Leila Choobineh

Department of Mechanical Engineering, SUNY Polytechnic Institute, Utica, NY 13502

# Bahgat Sammakia

Department of Mechanical Engineering, State University of New York at Binghamton, Vestal, NY 13850

### 1 Introduction

Portable hand-held electronic equipment has become inevitable in this digital era especially during the period of emerging remote workforce globally. Remote workforce demands heavy chip functionalities that require high graphics processing applications, namely, video conferencing. The merit of portable electronics such as tablets and smartphones is their compactness and uninterrupted operation. Uninterrupted operation of such portable devices requires uninterrupted power supply and device operating temperature below safe operating temperature. Uninterrupted power supply could be achieved by high capacity batteries. However, cooling is a more complex issue. For human comfort while using portable electronics, the temperature at the outside surface needs to be lower than 45 °C [1,2]. Thermal issues in small size electronics have been recognized and studied before [3–6]. To the authors' best knowledge, due to the limited space in the portable electronic devices, active cooling is not a viable option. Henceforth, an efficient passive cooling solution is required. Employing phase

responsiveness of the intermittent power load, Raghavan et al. [7] proposed a concept of computational sprinting where cores are activated to run for short time at the maximum power (thermal design power) and remain idle for some time till the user gives next input. The thermal design power is more than the cooling capacity of the system and the generated heat needs to be buffered. Thermal buffering has to be employed passively especially for portable electronics to store the heat during sprinting and release the heat during the idle duration to get ready for the next sprint. In this scenario of thermal buffering, the best candidate for the thermal energy storage is phase change material. The phase change material will be able to store the heat generated for short time by utilizing the heat as latent heat of fusion and releases that heat to ambient while the processor is idle. The PCM-based thermal energy storage systems involve heat storage by exploiting the high latent heat of the material. PCMs have a wide range of application in solar energy, aerospace, battery thermal management,

Contributed by the Electronic and Photonic Packaging Division of ASME for publication in the JOURNAL OF ELECTRONIC PACKAGING. Manuscript received December 30, 2020; final manuscript received July 26, 2021; published online September 24, 2021. Assoc. Editor: Jin Yang.

electronic cooling, etc. [8]. The major disadvantage of employing PCM is its low thermal conductivity. Most of the time, to enhance the thermal conductivity, thermal conductivity enhancers (TCEs) are employed in conjunction with the PCM. The TCEs are generally metal additions to the PCM in the form of foam, mesh, fins, solid nanoparticles, etc. [9].

During intermittent power surges, the system simultaneously demands a sufficiently high thermal conductivity and high energy storage capacity for safe operation. Theoretically, it is observed that the heat storage capacity and thermal conductivity of a composite are highly conflicting in nature. Considering a fixed volume of the composite of PCM and TCE, the addition of more TCE increases the effective thermal conductivity ( $k_{\rm eff}$ ) of the composite but simultaneously reduces the volume fraction of the PCM, which results in less amount of PCM available for melting and hence reduces the energy storage capacity ( $E_{\rm eff}$ ). Figure 1 shows an example of the variation of composite normalized thermal conductivity ( $k_{\rm eff}/k_{\rm TCE}$ ) and normalized energy storage capacity ( $E_{\rm eff}/k_{\rm TCE}$ ) with volume fraction of TCE. The effective energy storage capacity is calculated based on volume average. This tradeoff clearly indicates an optimal operating point for the heat sink.

The most common thermal energy storage-based heat sink used for cooling of electronic devices includes PCM embedded with porous foam. There are numerous studies that have been conducted to investigate the thermal performance of PCM-based heat sink with porous foam [10–12]. However, other arrangements of metal have been found to perform better. A study by Bentilla et al. [13] included experiments with various kinds of TCE arrangements such as wool, foam, and honeycomb of copper and aluminum. The authors found that honeycomb structure had the best performance among all. They concluded that having a high interfacial area between the metal and PCM and a low thermal resistance at base and metal TCE junction plays a very important role in thermal performance. Along with porous media and honeycomb structures, fins have also been a highly studied design. Srikanth and Balaji [14] studied the thermal performance of aluminum pin fins with n-eicosane heat sink and optimized the design by maximizing charging period and minimizing discharging period using Genetic Algorithm. Shatikian et al. [15] numerically studied the thermal energy storage system with vertical aluminum fins and PCM. They considered different fin thickness, height and gap between fins obtained the result in generalized form using dimensionless numbers. Typically, time taken to reach a set point temperature and time taken for system to cool down is considered to be the objective function in optimization of the design of the PCM and TCE composite.

However, in the case of intermittent power surges in portable electronics, the immediate response of the PCM and TCE composite becomes more important. This response has been quantified as a function of effective thermal conductivity and effective energy storage capacity of the system by Shamberger [16]. Shamberger introduced a term called cooling capacity figure of merit (FOM) to define the balance between the effective thermal conductivity and energy storage capacity. Following the cooling capacity figure of merit as the thermal performance parameter, Barako et al. [17] theoretically studied the optimization of a porous-PCM composite. They followed an effective thermal conductivity model for porous media developed by Hashin and Shtrikman [18] to find the optimal value of metal conductor volume fraction for a semi-infinite medium with planar heat source. They also found that the optimal metal volume fraction was 0.55 and that it was independent of the thermal conductivity ratio of porous metal to PCM after the ratio went beyond 100. Shamberger and Fisher [19] also found the optimal value of 0.5.

Most of the studies on thermal energy storage using PCM and TCE are based on large size of the composite, which cannot be the case for portable electronic devices given the space constraints. However, there are some studies performed for cooling of portable electronic devices. Shao et al. [20] did experiments by filling PCM in the well etched on the silicon substrate. They

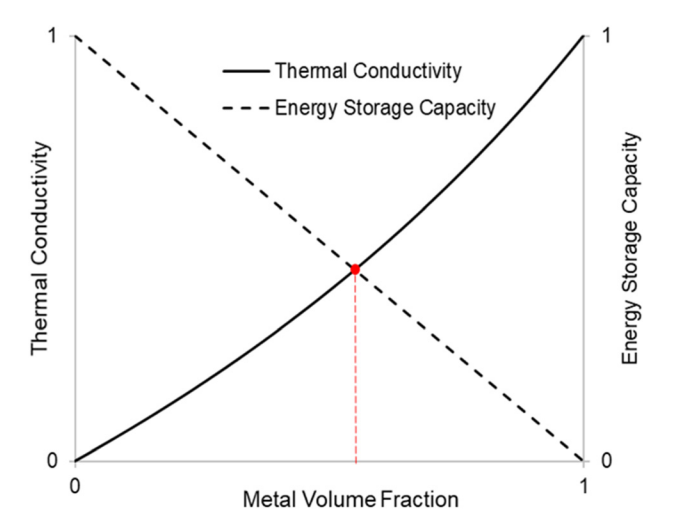


Fig. 1 Variation of normalized thermal conductivity and normalized energy storage capacity versus TCE volume fraction (for composite of copper and *n*-octadecane)

focused on finding the temperature time history for computational sprinting concept. They supplied a heat input of around 11 W for 0.6 s and turned off the heater to allow the PCM to cool and be ready for the next thermal spike. Ahmed et al. [21] also performed experiments using PCM for mobile phone cooling. They considered a 2 mm thick PCM packed in an aluminized film and placed it on the top of a heater. They did experiments at three different heat input of 4 W, 6 W, and 8 W and found that the temperature at the back cover of the phone was maintained below  $70\,^{\circ}\mathrm{C}$  even at 8 W continuous heat input for  $30\,\mathrm{min}$ .

As evidenced by the literature review, there is need of studies that rely upon a simplified numerical model to optimize a PCMbased heat sink design. The objective of this study is to numerically investigate the effect of thermal conductivity enhancement of a PCM-based composite and quantify the optimal effective thermal conductivity that maximizes the heat sink FOM. The present study focuses on investigating different volume fraction of the TCE for a fixed total volume of the composite for a morphology for which effective thermal conductivity is not available through existing models and needs to be found. The TCE structure in present study comprises vertical fins along with one horizontal fin to cover a broad range of volume fraction. In this study, a direct model as well as a simplified model was used to compare different volume fractions. To find the thermal performance behavior as a function of volume fraction alone, other constraints such as fixed area of contact between TCE and PCM and fixed thickness of the TCE are added.

## 2 Numerical Analysis

**2.1 Direct Model.** Figure 2 shows the schematic of the problem under consideration. The computational domain consists of a cuboidal heat sink with a height and width of 1 mm and 25 mm, respectively [21]. The third dimension into the plane is 25 mm. Base area is used only to calculate the heat flux. The bottom base had a uniform heat input of 10 W, which translates to a flux of 1.6 W/cm<sup>2</sup> [20,21]. The side walls are set as adiabatic and the boundary condition at the top wall is considered as a uniform heat transfer coefficient of 10 W/m<sup>2</sup>K with an ambient temperature of 300 K.

For detailed numerical study, four different volume fractions of TCE ( $\varphi$ ) were selected in the range 0.38–0.7. Furthermore, three materials were selected as TCEs and three PCMs were chosen. All the PCMs were selected with different thermal conductivity and different latent heat of fusion and almost same melting point. It was made sure that all the PCMs had the melting point below

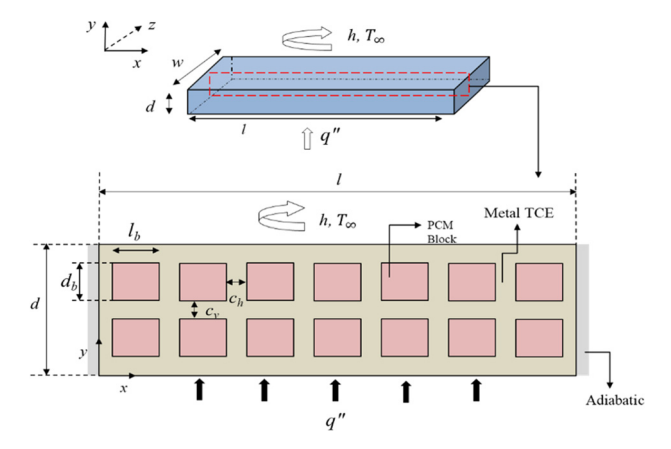


Fig. 2 Problem definition: two-dimensional computational domain (detailed dimensions of TCE and PCM enclosed are given in Table 1)

 $45\,^{\circ}\mathrm{C}$  [1,2]. The materials selected and their properties are shown in Tables 2 and 3.

The constraints on the heat sink geometry are as follows:

- (1) The interfacial area between the TCE and PCM was kept the same for all the four volume fractions of TCE.
- The thicknesses c<sub>v</sub> and c<sub>h</sub> were both the same and equal for all the cases.
- (3) Total volume of the heat sink was fixed. The gap between the fins and total number of fins (N) were varied to make designs for different volume fractions. Details about the dimensions for different volume fractions are shown in Table 1 and Fig. 2.

# **2.2** Governing Equations for Direct Model. For the TCE, the conduction equation is solved

$$\frac{\partial}{\partial t}(\rho_s C_p T) = \frac{\partial}{\partial x_i} \left( k_s \frac{\partial T}{\partial x_i} \right) \tag{1}$$

For the PCM section, two-dimensional governing equations are solved along with enthalpy porosity scheme for melting using ANSYS FLUENT 19.2.

Continuity equation

$$\frac{\partial \rho}{\partial t} + \rho(\nabla \cdot \mathbf{v}) = 0 \tag{2}$$

Momentum equations

$$\frac{\partial \mathbf{v}}{\partial t} + \mathbf{v} \cdot \nabla \mathbf{v} = -\frac{1}{\rho} \nabla P + \nu \nabla^2 \mathbf{v} + \mathbf{g} + S \tag{3}$$

Energy equation

$$\frac{\partial}{\partial t} (\rho \hat{h}) + \nabla \cdot (\rho v \hat{h}) = \nabla \cdot (k \nabla T) \tag{4}$$

Table 2 Thermophysical properties of TCEs used

Material	Copper	Aluminum	Silicon
Thermal conductivity (W/mK) Specific heat (J/kgK) Density (kg/m³)	387.6	202.4	148
	381	871	710
	8978	2719	2330

Table 3 Thermophysical properties of phase change materials used [8,9]

Material	<i>n</i> -octadecane	LiNO <sub>3</sub> –3H <sub>2</sub> O	CaCl <sub>2</sub> –6H <sub>2</sub> O
Thermal conductivity (W/mK)	0.25 <sup>a</sup>	0.58	1.088
Density (kg/m <sup>3</sup> )	771	1460	1650
Latent heat (kJ/kgK)	243.5	256	195
Melting temperature (°C)	27.7	30	29.5
Specific heat (J/kgK)	2222	2760	1420

<sup>&</sup>lt;sup>a</sup>Property is average of solid and liquid.

Here, specific enthalpy h is the sum of sensible enthalpy and the latent heat

$$\hat{h} = \hat{h}_s + \hat{h}_l \tag{5}$$

$$\hat{h}_s = \hat{h}_{\text{ref}} + \int_{T_{\text{ref}}}^T c_p dT \tag{6}$$

$$\hat{h}_l = \gamma L \tag{7}$$

where L is the latent heat of the PCM and  $\gamma$  is the liquid fraction, which varies in the range of 0–1 for the given melting range of the PCM from solidus temperature  $T_{\rm sol}$  to liquidus temperature  $T_{\rm liq}$ . The liquid fraction  $\gamma$  is defined as

$$\gamma = 0 \text{ if } T < T_s \tag{8}$$

$$\gamma = 1 \text{ if } T > T_l \tag{9}$$

$$\gamma = \frac{T - T_{\text{sol}}}{T_{\text{liq}} - T_{\text{sol}}} \text{ if } T_{\text{sol}} \le T \le T_{\text{liq}}$$
 (10)

In the enthalpy porosity technique, by Voller and Prakash [22], the mushy zone is treated as a porous media with porosity in a cell equal to the liquid fraction of the melt PCM in the cell. They defined a porosity function  $A(\gamma)$  to incorporate the porous media flow similar to the Carman–Kozeny equations [22] for fluid flow in porous media. The source term S is shown in the momentum equation (Eq. (4)) given by the following relation:

$$S = -A(\gamma)v = -C\frac{(1-\gamma)^2}{(\varepsilon+\gamma^3)}v \tag{11}$$

where  $\varepsilon$  is a small number equal to 0.001 to avoid division by zero and C is a constant. The value of C is usually taken in the range

Table 1 Dimensions for different volume fraction

		Gap bet	Gap between fins		ickness	
Design	Volume fraction $(\varphi)$	$l_b$ mm	$d_b  \mathrm{mm}$	$c_v$ mm	$c_h  \mathrm{mm}$	Number of vertical fins (N)
1	0.7	0.15	0.25	0.1	0.1	201
2	0.61	0.2	0.3	0.1	0.1	165
3	0.48	0.3	0.35	0.1	0.1	125
4	0.38	0.375	0.4	0.1	0.1	105

 $10^4$ – $10^7$ . The value of C was  $10^6$  for this study though there is no significant effect of the C value on the results.

The above governing equations were numerically solved using the commercially available solver ansys fluent 19.2. The grid size was chosen to be  $0.01\,\mathrm{mm}$  and time-step set as  $0.01\,\mathrm{s}$  after doing the independency study. The convergence criteria were  $10^{-6}$  for velocity and continuity, and  $10^{-9}$  for energy.

- **2.3 One-Dimensional Effective Model.** For modeling the PCM-TCE composite, effective thermophysical properties of the composite were used. A single energy equation was solved for the composite with a source term for melting/solidification. The following assumptions were considered for the composite medium:
  - (1) The properties of respective phases remain constant throughout the temperature range considered.
  - (2) Solid and liquid densities are independent of temperature.
  - (3) Natural convection in the melt liquid is neglected (Fig. 3).

The governing equation for the composite can be written as

$$(\rho c_p)_{\text{eff}} \frac{\partial T}{\partial t} = \nabla . (k_{\text{eff}} \nabla T) - \rho [(c_{pl} - c_{ps})T + L] \frac{\partial f}{\partial t}$$
 (12)

$$f = \begin{cases} 0 & T < T_m - \varepsilon \\ \frac{1}{T - T_m + \varepsilon} & T > T_m + \varepsilon \\ \frac{T - T_m + \varepsilon}{2\varepsilon} & (T_m - \varepsilon) \le T \le (T_m + \varepsilon) \end{cases}$$
(13)

where f is the liquid fraction of PCM. The second term in the right-hand side of Eq. (12) is the source term for melting/solidification [23].

Furthermore, the one-dimensional governing equation was solved using a finite difference technique with central differencing scheme for spatial discretization in diffusion term and Crank Nicolson scheme for time marching. The liquid fraction was considered in the range 0-1 as a linear function of temperature in the melting region. A small number  $\varepsilon$  was considered to avoid the sudden change of liquid fraction from 0 to 1. The solution was obtained by developing a code using MATLAB R2019. The code was validated against the analytical solution available for the Stefan problem shown in Fig. 4. The Stefan problem considered was melting of the semi-infinite medium which is at an initial temperature ( $T_{\rm initial}$ ) at time t < 0. At t = 0, temperature at x = 0 is increased to a higher temperature ( $T_{\rm H}$ ). A PCM material was

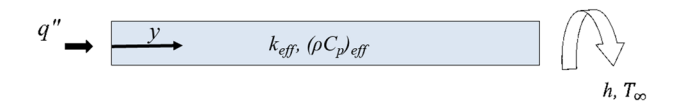


Fig. 3 One-dimensional computational domain for effective model

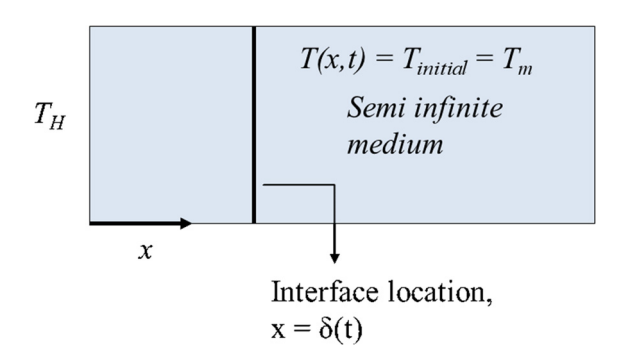


Fig. 4 Stefan problem used for validation

considered to validate the code with the domain completely filled with just the PCM. The Stefan number was 0.18.

The analytical solution [24] for the Stefan problem is

$$\frac{T(x < \delta(t), t) - T_H}{(T_{\text{initial}} - T_H)} = \begin{cases} erf \frac{x}{2\sqrt{(k/\rho C_p)t}} \\ erf(\lambda) \end{cases}$$
(14)

$$T(x > \delta(t), t) = T_{\text{initial}}$$
 (15)

where  $\delta(t)$  is interface location at time t. Interfacial location is determined from following expression:

$$\delta(t) = 2\lambda \sqrt{\frac{k}{\rho C_p}} t \tag{16}$$

 $\lambda$  is obtained by solving for the root of the following transcendental equation:

$$\lambda e^{\lambda^2} \operatorname{erf}(\lambda) = \frac{\operatorname{Ste}}{\sqrt{\pi}} \tag{17}$$

Figure 5 shows the validation of the code developed.

### 3 Results and Discussions

3.1 Effective Thermal Conductivity and Effective Energy Storage Capacity. Assuming that the energy storage is predominantly in the form of latent heat, the effective energy storage for a composite can be expressed as a function of the proportion of the PCM that is available for melting. Here,  $L_{\rm PCM}$  is the latent heat of the PCM

$$E_{\rm eff} = L_{\rm PCM}(1 - \varphi) \tag{18}$$

The benchmarked effective model (discussed in Sec. 2.3) was used to find the approximate value of the effective thermal conductivity ( $k_{\text{eff}}$ ) for all the TCE–PCM composite designs shown in Table 1. First and foremost, for each case, the temperature gradient  $(\Delta T/d)$  in the composite and the base temperature time histories were obtained from the direct model shown in Sec. 3.2. Then, the one-dimensional effective model was used to determine the approximate value of the composite  $k_{\rm eff}$  that gives the same temperature gradient as obtained from the direct model for each design points.  $\Delta T$  is the temperature difference between the top (y = 1 mm) and bottom point (y = 0) of the heat sink at the midlength (x = 12.5 mm). The approximate value of  $k_{\rm eff}$  was obtained by minimizing the mean absolute error (MAE) of the temperature gradient for both the models in the melting region by iteratively changing the value of  $k_{\rm eff}$ . The iterations were stopped when MAE reached 0.01

$$MAE = \frac{1}{t} \sum_{i=1}^{t} |T_{g,i} - \hat{T}_{g,j}|$$
 (19)

An initial guess of the  $k_{\rm eff}$  was obtained by calculating the  $k_{\rm eff}$  for the composite from the series combination model [25] of TCE and PCM. The time-step and grid size were 0.01 s and 0.1 mm.

Figure 6 shows the temperature gradient–time history obtained for both the models using Copper, Aluminum, and Silicon with *n*-octadecane.

The effective thermal conductivity was obtained for all the combinations of TCE, PCM, and volume fractions. Figure 7 shows the variation of  $k_{\rm eff}$  and  $E_{\rm eff}$  for n-octadecane.

Another set of investigations were performed with two other PCMs, LiNO<sub>3</sub>–3H<sub>2</sub>O, and CaCl<sub>2</sub>–6H<sub>2</sub>O, whose properties are shown in Table 3. Among the three PCMs considered, the

maximum PCM thermal conductivity was 1.08 W/mK (CaCl<sub>2</sub>-6H<sub>2</sub>O). It can be observed from Tables 2 and 3 that the thermal conductivity of the PCM  $(k_{PCM})$  was much smaller than the thermal conductivity of TCEs ( $k_{TCE}$ ). Upon numerical investigation with both the models for all the material combinations, it was evident that the major contribution to the composite effective thermal conductivity stemmed from the volume fraction and thermal conductivity of just the TCE, while PCM had a negligible effect on the composite effective thermal conductivity as shown in Fig. 8. Henceforth,  $k_{\rm eff}$  was considered to be dependent only on the  $k_{\text{TCE}}$  and  $\varphi$ . This assumption holds good only for the cases of PCM that have very small thermal conductivities (ex. paraffins). To find the optimal value of  $\varphi$ , the effective thermal conductivity results obtained for *n*-octadecane (shown in Fig. 7) were normalized with respect to the thermal conductivity of pure TCE. When the effective thermal conductivity for each TCE was normalized to obtain the normalized  $k_{\rm eff}$  just as a function of TCE volume fraction

$$\widetilde{k_{\text{eff}}} = \frac{k_{\text{eff}}}{k_{\text{TCE}}} = f(\varphi)$$
 (20)

**3.2 Figure of Merit.** Following the work by Shamberger [16], a term figure of merit was employed to determine the balance between the effective thermal conductivity and effective

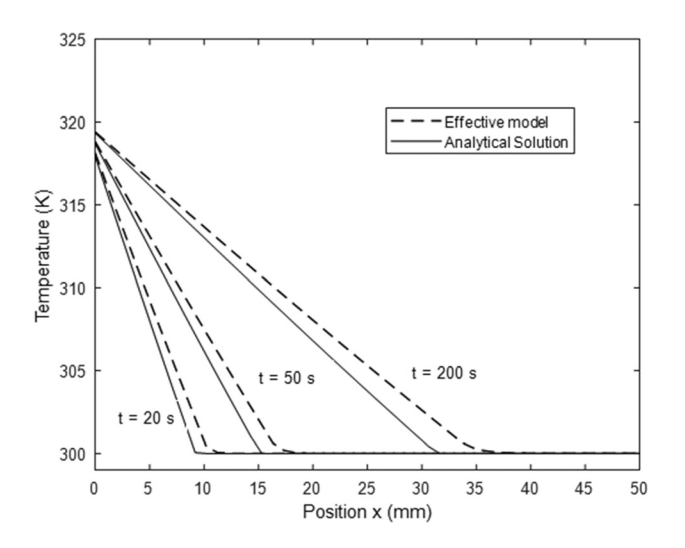


Fig. 5 Validation of the code with the Stefan problem (Ste = 0.18)

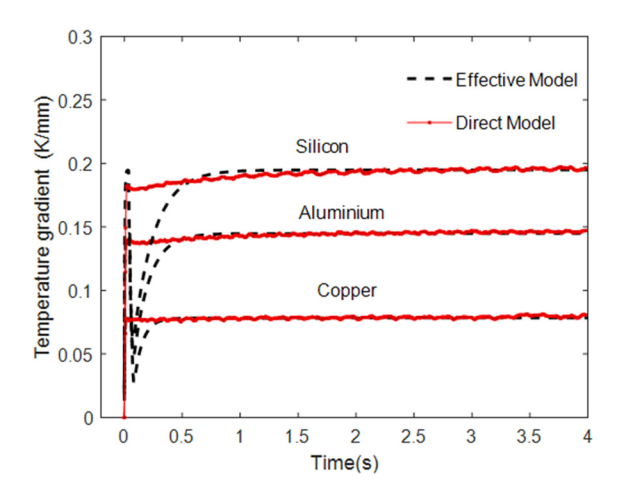


Fig. 6 Comparison of temperature gradient-time history of both models for *n*-octadecane at TCE volume fraction of 0.48

energy storage. The FOM based on the effective properties of the composite can be defined as (Fig. 9)

$$\eta_{\rm eff} = \sqrt{k_{\rm eff} E_{\rm eff}}$$
(21)

In the above equation,  $k_{\rm eff}$  and  $E_{\rm eff}$  are obtained from Eqs. (18) and (20). The value of  $\eta_{\rm eff}$  can be written as

$$\eta_{\text{eff}} = \sqrt{k_{\text{TCE}}L_{\text{PCM}}(1-\varphi) \cdot f(\varphi)}$$
(22)

 $\eta_{\rm eff}$  was plotted for all three TCEs with n-octadecane as the PCM in Fig. 10. It can be observed that the optimal value of  $\varphi$  is almost the same for all the TCEs and n-octadecane combinations. Since, the thermal conductivity of PCM is now playing major role and difference in the PCMs considered is only in latent heat of fusion, it is evident that the figure of merit curve will change if some other PCM is used instead of n- octadecane but maxima will always be at the same value of metal volume fraction. So, following Eq. (23), the figure of merit would be different and dependent on the thermal conductivity of the TCE and latent heat of the PCM.

In Eq. (23),  $\eta_{\rm eff}$  can be made dimensionless to find the optimal point

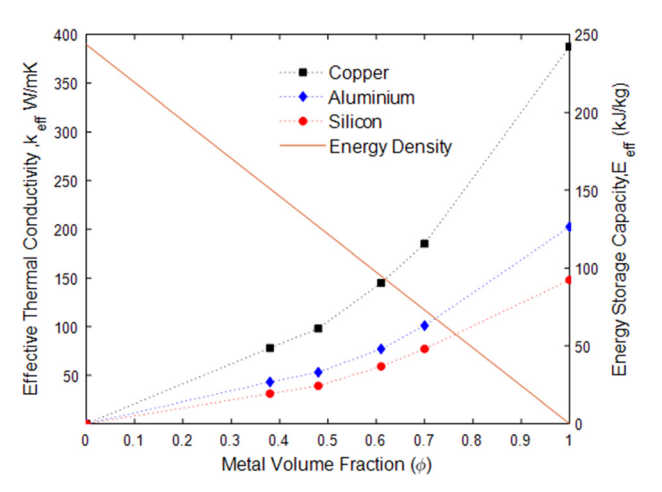


Fig. 7 Effective thermal conductivity and effective energy storage capacity for different TCEs and different volume fraction for *n*-octadecane

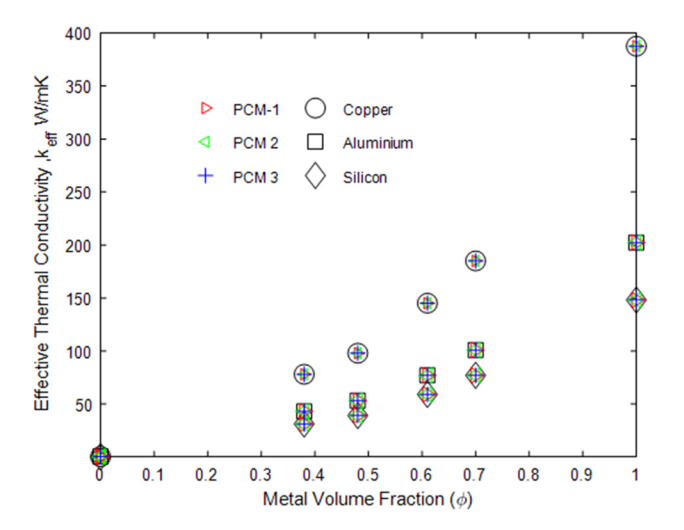


Fig. 8 Effective thermal conductivities for different TCE and PCM combinations (PCM-1: n-octadecane, PCM-2: LiNO<sub>3</sub>-3H<sub>2</sub>O, and PCM-3: CaCl<sub>2</sub>-6H<sub>2</sub>O)

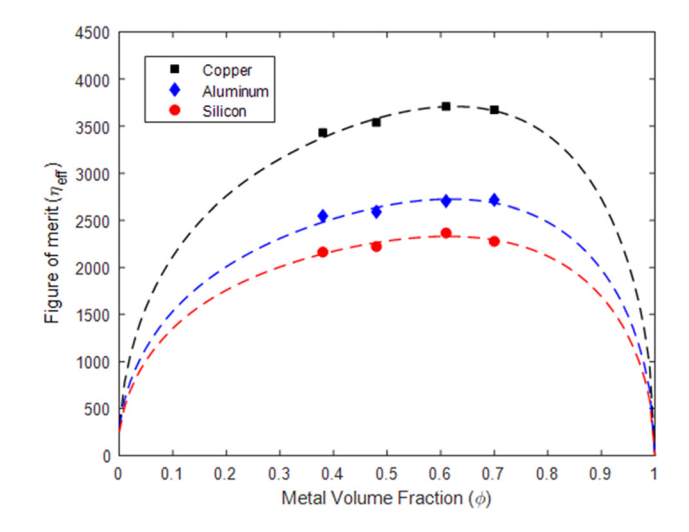


Fig. 9 Figure of merit obtained for all TCEs and n-octadecane

$$\widetilde{\eta_{\rm eff}} = \frac{\eta_{\rm eff}}{\sqrt{k_{\rm TCE}L_{\rm PCM}}} = \sqrt{(1-\varphi) \cdot f(\varphi)}$$
 (23)

After substituting  $f(\varphi)$  from Eq. (21) in the above equation,  $\widetilde{\eta_{\rm eff}}$  was differentiated and made equal to zero. The positive root obtained after solving was  $\varphi \approx 0.64$ . The value was found to be in near agreement to the optimal volume fraction of 0.55 for a porous media obtained by Barako et al. [17].

3.3 Comparison With Other Models. The effective thermal conductivity obtained for the copper and n-octadecane composite design used in this work was compared with the effective conductivity obtained from existing effective models for PCM-porous media composite [18,25,26] as shown in Table 4 and Fig. 10. The results make it evident that effective thermal conductivity values were around 20–30% less than the values obtained from the Hashin-Shtrikman porous media model [18] for Copper n-octadecane composite. The disparity is mainly attributed to the higher area of contact between the TCE and PCM in the case of porous media [13]. Furthermore, the maximum value of  $\eta_{\rm eff}$  in the present design was 15.1% lower than that of porous metal at  $\varphi=0.55$  using the Hashin-Shtrikman model.

The maximum FOM at minimum metal volume fraction of 0.5 was obtained for parallel arrangement [25]. However, for the morphology considered in the present study, the maximum FOM was

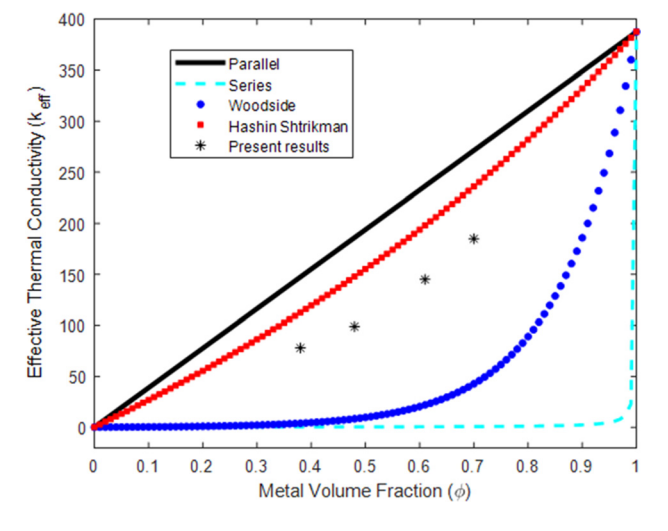


Fig. 10 Effective thermal conductivity obtained for copper and *n*-octadecane for different models and present results

Table 4 Expression of effective thermal conductivity for different models

Model	Expression $(k_{\text{eff}})$
Parallel [25]	$\varphi k_{\text{TCE}} + (1 - \varphi) k_{\text{PCM}}$
Series [25]	$\frac{k_{\text{PCM}} k_{\text{TCE}}}{\varphi k_{\text{PCM}} + (1 - \varphi) k_{\text{TCE}}}$
Woodside [26]	$k_{ ext{PCM}}^{1-arphi}k_{ ext{TCE}}^{arphi}$
Hashin Shtrikman [18]	$k_{\text{TCE}} \left[ 1 + \frac{3(k_{\text{PCM}} - k_{\text{TCE}})(1 - \varphi)}{3k_{\text{TCE}} + (k_{\text{PCM}} - k_{\text{TCE}})\varphi} \right]$

obtained for a metal volume fraction of 0.65. It is also to be noted that for the theoretical effective thermal conductivity for parallel model is based on considering the composite as coherent and demands a critical length scale of fin thickness and gap between fins for the relation to be valid [19]. The authors would like to recommend that future optimization studies on PCM-TCE composite should consider morphology (benchmarked with parallel arrangement) to maximize FOM at minimum metal volume fraction [27].

## **Conclusions**

A simplified effective thermal conductivity model was developed to simulate the phase change heat transfer and estimate the effective thermal conductivity of the composite. PCM-metal composite with PCM added into the metal honeycomb as a potential heat transfer medium was considered in this study. A direct computation fluid dynamics model was used as a benchmarking tool for the present effective model in the paper. The effective thermal conductivity obtained from the simplified model was used to determine the FOM. The thermal performance was evaluated by employing the figure of merit to determine the optimal value of the TCE volume fraction in the composite. For  $k_{PCM} \le 1$ , the optimal volume fraction of TCE was found to be same for all the TCE materials and the optimum value was  $\varphi = 0.64$ . It was observed on comparison of present design (copper and n-octadecane composite) with the effective thermal conductivity model for porous media that present design had  $k_{\rm eff}$  20–30% (depending upon the volume fraction) lesser than the  $k_{\rm eff}$  of the porous TCE and PCM. Furthermore, the maximum figure of merit for present design was approximately 15% less than that of the Hashin-Shtrikman model. Among all the models compared, the figure of merit was maximum for parallel combination of PCM and TCE at minimal metal volume fraction. The morphology in the present design achieves 23% lesser maximum FOM at 26% higher metal volume fraction compared to parallel combination.

# **Funding Data**

- Semiconductor Research Corporation (SRC) (Grant No. GRC TASK 2878.015; Funder ID: 10.13039/100000028).
- SUNY Research Foundation.

### Nomenclature

c = gap between fins (mm)

 $c_p$  = specific heat at constant pressure (J/kgK)

d = height

e = energy storage capacity (J/kg)

f =liquid fraction (effective model)

 $h = \text{heat transfer coefficient } (\text{W/m}^2\text{K})$ 

 $\hat{h} = \text{enthalpy (J/kg)}$ 

k = thermal conductivity (W/mK)

l = length (m)

L = latent heat (J/kg)

N = number of vertical fins

 $q'' = \text{heat flux (W/m}^2)$ 

- Ste = Stefan number  $(c_p \Delta T/L)$ 
  - t = time (s)
  - T = temperature (K)
  - v = velocity component (m/s)
  - w = width (m)
  - x = x-coordinate (m)
  - y = y-coordinate (m)

### **Greek Symbols**

- $\gamma$  = liquid fraction
- $\delta$  = interface location (m)
- $\Delta = difference$
- $v = \text{kinematic viscosity (m}^2/\text{s})$
- $\rho = \text{density (kg/m}^3)$
- $\varphi$  = volume fraction of TCE

### Subscripts

- b = PCM block
- eff = effective property
- g = gradient
- h = horizontal
- i = component
- l = liquid
- liq = liquidus
- m = melting temperature
- ref = reference
- s = solid
- sol = solidus
- v = vertical

### References

- [1] Patapoutian, A., Peier, A. M., Story, G. M., and Viswanath, V., 2003, 'ThermoTRP Channels and Beyond: Mechanisms of Temperature Sensation," Nat. Rev. Neurosci., 4(7), p. 7.
- [2] Greenspan, J. D., Roy, E. A., Caldwell, P. A., and Farooq, N. S., 2003, "Thermosensory Intensity and Affect Throughout the Perceptible Range," Somatosens. Mot. Res, 20(1), pp. 19-26.
- [3] Choobineh, L., and Jain, A., 2013, "Determination of Temperature Distribution in Three-Dimensional Integrated Circuits (3D ICs) With Unequally-Sized Die,
- Appl. Therm. Eng, **56**(1–2), pp. 176–184. [4] Rangarajan, S., Hadad, Y., Choobineh, L., and Sammakia, B., Jun. 2020, "Minimizing Temperature Nonuniformity by Optimal Arrangement of Hotspots in Vertically Stacked Three-Dimensional Integrated Circuits," ASME J. Electron. Packag., 142(4), p. 041109.
- [5] Choobineh, L., and Jain, A., 2015, "An Explicit Analytical Model for Rapid Computation of Temperature Field in a Three-Dimensional Integrated Circuit (3D IC)," Int. J. Therm. Sci, 87, pp. 103–109.
- [6] Choobineh, L., and Jain, A., 2012, "Analytical Solution for Steady-State and Transient Temperature Fields in Vertically Stacked 3-D Integrated Circuits," IEEE Trans. Compon. Packag. Manuf. Technol, 2(12), pp. 2031-2039.

- [7] Raghavan, A., Luo, Y., Chandawalla, A., Papaefthymiou, M., Pipe, K. P., Wenisch, T. F., and Martin, M. M., 2012, "Computational Sprinting," IEEE International Symposium on High-Performance Comp Architecture, New Orleans, LA, Feb. 25–29, pp. 1–12.
- [8] Fan, L., and Khodadadi, J. M., 2011, "Thermal Conductivity Enhancement of Phase Change Materials for Thermal Energy Storage: A Review," Renew. Sustainable Energy Rev., 15(1), pp. 24–46.
- [9] Pereira da Cunha, J., and Eames, P., 2016, "Thermal Energy Storage for Low and Medium Temperature Applications Using Phase Change Materials—A Review," Appl. Energy, 177, pp. 227–238.
  [10] Zhou, D., and Zhao, C. Y., 2011, "Experimental Investigations on Heat Trans-
- fer in Phase Change Materials (PCMs) Embedded in Porous Materials," Appl. Therm. Eng, 31(5), pp. 970–977.
- [11] Liu, Z., Yao, Y., and Wu, H., 2013, "Numerical Modeling for Solid-Liquid Phase Change Phenomena in Porous Media: Shell-and-Tube Type Latent Heat
- Thermal Energy Storage," Appl. Energy, 112, pp. 1222–1232.
  [12] Zhang, P., Meng, Z. N., Zhu, H., Wang, Y. L., and Peng, S. P., 2017, "Melting Heat Transfer Characteristics of a Composite Phase Change Material Fabricated by Paraffin and Metal Foam," Appl. Energy, 185, pp. 1971–1983.
- [13] Bentilla, E. W., Karre, L. E., and Sterrett, R. F., 1966, "Research and Development Study on Thermal Control by Use of Fusible Materials Final Report," NASA, Washington, DC.
- [14] Srikanth, R., and Balaji, C., 2017, "Experimental Investigation on the Heat Transfer Performance of a PCM Based Pin Fin Heat Sink With Discrete Heating," Int. J. Therm. Sci, 111, pp. 188-203.
- [15] Shatikian, V., Ziskind, G., and Letan, R., 2008, "Numerical Investigation of a PCM-Based Heat Sink With Internal Fins: Constant Heat Flux," Int. J. Heat Mass Transfer, 51(5-6), pp. 1488-1493.
- [16] Shamberger, P. J., 2015, "Cooling Capacity Figure of Merit for Phase Change Materials," ASME J. Heat Transfer, 138(2), p. 024502.
- [17] Barako, M. T., Lingamneni, S., Katz, J. S., Liu, T., Goodson, K. E., and Tice, J., 2018, "Optimizing the Design of Composite Phase Change Materials for
- High Thermal Power Density," J. Appl. Phys, **124**(14), p. 145103.
  [18] Hashin, Z., and Shtrikman, S., 1962, "A Variational Approach to the Theory of the Effective Magnetic Permeability of Multiphase Materials," J. Appl. Phys, 33(10), pp. 3125-3131.
- [19] Shamberger, P. J., and Fisher, T. S., 2018, "Cooling Power and Characteristic Times of Composite Heatsinks and Insulants," Int. J. Heat Mass Transfer, 117, pp. 1205-1215.
- [20] ShaoRaghavan, L., Emurian, A. L., Papaefthymiou, M. C., Wenisch, T. F., Martin, M. M., and and Pipe, K. P., 2014, "On-Chip Phase Change Heat Sinks Designed for Computational Sprinting," Semiconductor Thermal Measurement and Management Symposium (SEMI-THERM), San Jose, CA, Mar. 9–13, pp. 29-34.
- Ahmed, T., Bhouri, M., Groulx, D., and White, M. A., 2018, "Passive Thermal Management of Tablet PCs Using Phase Change Materials: Continuous Operation," Int. J. Therm. Sci., 134, pp. 101-115.
- Voller, V. R., and Prakash, C., 1987, "A Fixed Grid Numerical Modelling Methodology for Convection-Diffusion Mushy Region Phase-Change Problems," Int. J. Heat Mass Transfer, 30(8), pp. 1709-1719.
- [23] Simpson, J. E., Garimella, S. V., and de Groh, H. C., 2002, "Experimental and Numerical Investigation of the Bridgman Growth of a Transparent Material," J. Thermophys. Heat Transfer, 16(3), pp. 324–335.
- [24] Dantzig, J. A., 1989, "Modelling Liquid-Solid Phase Changes With Melt Con-
- vection," Int. J. Numer. Methods Eng. 28(8), pp. 1769–1785.
  [25] Tavman, I. H., 1996, "Effective Thermal Conductivity of Granular Porous Materials," Int. Commun. Heat Mass Transfer, 23(2), pp. 169–176.
- Woodside, W., and Messmer, J. H., 1961, "Thermal Conductivity of Porous Media. I. Unconsolidated Sands," J. Appl. Phys, **32**(9), pp. 1688–1699.
- Rangarajan, S., and Balaji, C., 2019, Phase Change Material-Based Heat Sinks: A Multi-Objective Perspective, CRC Press, Boca Raton, FL.